PCCP

Accepted Manuscript

ROYAL SOCIETY OF CHEMISTRY

www.rsc.org/pccp

Graphical abstract Part II

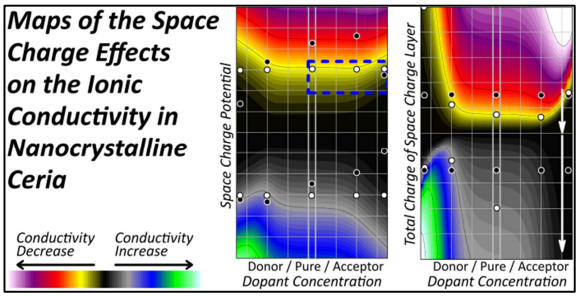

The features of space charge profiles and their dependencies are investigated in detail; arising prospects and limitations for applications are discussed.

Numerical Calculations of Space Charge Layer Effects in Nanocrystalline Ceria. Part II: Detailed Analysis of the Space Charge Layer Properties

Marcus C. Göbel, Giuliano Gregori,[I] Joachim Maier

Max Planck Institute for Solid State Research, Heisenbergstr. 1, D-70569 Stuttgart, Germany

Abstract

The numerical approach presented in Part I is used to investigate in detail some important characteristics of space charge layer (SCL) concentration profiles (steepness, extent, charge contributions and total charge), which determine the resulting SCL effects on the ionic and electronic transport. Here, as a case study the conductivity changes in nanocrystalline ceria are discussed over a broad range of dopant concentration (acceptor and donor-doped) as well as space charge potential values. In addition, the effects of a mobile dopant on the SCL charge carrier profiles are addressed. Finally, using the numerical approach the possibilities of adjusting (under realistic conditions) the SCL effects to improve the conduction properties of nanocrystalline CeO_2 are discussed.

[I] Corresponding author
E-mail address: g.gregori@fkf.mpg.de, s.weiglein@fkf.mpg.de
Fax: +49-711-689-1722

1. Introduction

In the first part of the study[1], we presented a numerical approach to solve the Poisson-equation of the charge carrier concentration profiles for one-dimensional, non-overlapping space charge layers (SCLs), which was then used in the case of nanocrystalline cerium oxide (CeO_2). After having verified the reliability of the numerical calculations, it was shown that compared with the usual analytical approximation, the numerical approach allows for an accurate determination of the charge carrier concentration SCL profiles not only in the Gouy-Chapman and Mott-Schottky cases but, remarkably, also in the more complex, so-called mixed situations.

The purpose of the second part of the study is to employ the numerical calculation to gain further insights on the space charge layers properties and on their effects on the ionic and electronic transport.[II] This contribution is hence organized as follows: First, the calculations are used to study in detail the main features of the SCLs without any assumption *a priori* regarding the spatial distribution of the mobile charge carriers. This section includes (i) the determination of which mobile charge carrier contributes most to the compensation of the grain boundary core charge Σ_{Core} depending on SCL potential Φ_0 and dopant concentration; (ii) the assessment of the space charge steepness α and the space charge extent ℓ_{SCL}; and (iii) the analysis of the SCL profiles (and their impact on the conduction properties) in the case of a mobile dopant (at equilibrium).

In the second part of this contribution, the numerical calculations are used to examine realistic scenarios - particularly in terms of Σ_{Core} (or Σ_{SCL}) - for adjusting the space charge effects to improve the electrical transport. It is worth recalling that, since SCL effects have a considerable impact on the conduction properties, there have been several attempts to modify Φ_0 with the aim of modifying the electrical conductivity[2-5]. Particularly interesting is the case of boron-decorated CeO_2[4], in which the improved electronic conductivity (a factor 10 larger than undoped CeO_2 at 500°C) could be quantitatively explained by an increase of the positive Φ_0. Here, we focus our attention on the ionic transport and show that although the adjustments of Σ_{core} (or Σ_{SCL}) are in some cases (i.e. heavily doped CeO_2) rather limited, the resulting beneficial effects on the conductivity can yet be extremely favorable for technological applications.

[II] Here, the same parameters used in first part of this study are employed (see Table 2 of Part I), namely $n_\infty = 2 \cdot 10^{18}$ cm^{-3}, $T = 973$ K, $pO_2 = 10^{-10}$ bar, $\varepsilon_r = 26$ and $d = 40$ nm. Please refer to Table 1 for the definition of the parameters.

Table 1 Definition of the physical quantities used in the present study. Note that in this contribution the subscript *0* generally denotes the coordinate $x = 0$, i.e. the position adjacent to the interface (e.g. Φ_0 is the electric potential at the interface). The subscript ∞ denotes the bulk of the material.

Variables	***Description***
$c_{A'}$	acceptor dopant concentration ($z_{A'} = -1$)
c_{Ce}	concentration of the cerium cations in CeO_2
$c_{D^\bullet}$	donor dopant concentration ($z_{D^\bullet} = 1$)
c_i , $c_{i,x}$	concentration of mobile charge carrier *i* (at coordinate x)
$c_{IM,j}$	bulk concentration of immobile charge carrier *j*
$c_{i,\infty}$	bulk concentration of mobile charge carrier *i*
c_∞	bulk concentration
$c_{V_O^{\bullet\bullet},\infty}$	oxygen vacancy bulk concentration
d	grain size
e	elementary charge ($1.60217648 \cdot 10^{-19}$ C)
E , E_x	electric field (at coordinate *x*)
i	counter variable for mobile charge carriers
s_m	normalized effectively measured conductivity (including parallel and perpendicular boundary contributions)
$s_{i,m}$	normalized effectively measured conductivity of the charge carrier i (including parallel and perpendicular boundary contributions)
j	counter variable for immobile charge carriers
k	counter variable for calculation steps
k_B	Boltzmann constant ($1.380648 \cdot 10^{-23}$ J/K)
ℓ_{SCL}	combined length of the SCL
n_∞	electron bulk concentration
N_{IM}	number of immobile charge carriers
N_M	number of mobile charge carriers
pO_2	oxygen partial pressure
r	criterion to define the SCL length (percentage of charge Σ_i (or Ω_i) inside a SCL of certain length)
T	temperature in Kelvin
x , x_k	distance from boundary (at calculation step *k*)
x_ρ	coordinate of charge balance point
$z_{IM,j}$	charge number of immobile charge carrier *j*
α	SCL steepness
ε_r	relative permittivity
θ	temperature in °C
λ	Debye length
λ^*	screening length (Mott-Schottky case)
$\lambda_{e'}$	Debye length (concerning e' bulk concentration)
$\lambda_{V_O^{\bullet\bullet}}$	Debye length (concerning $V_O^{\bullet\bullet}$ bulk concentration)
σ_m	total effectively measured conductivity (including parallel and perpendicular boundary contributions)

$\sigma_{i,m}$	total effectively measured conductivity of charge carrier *i* (including parallel and perpendicular boundary contributions)
$\sigma_{i,\infty}$	bulk conductivity of charge carrier *i*
σ_{∞}	bulk conductivity
ρ , ρ_x	(3-dimensional) charge density (at coordinate *x*)
ρ_{IM}	charge density contribution of immobile charge carriers
$\Sigma_{A'}$	charge contribution due to the enrichment (or depletion) of the mobile acceptor dopant
Σ_{Core}	GB core charge
$\Sigma_{D^{\bullet}}$	charge contribution due to the enrichment (or depletion) of the mobile donor dopant
Σ_{Dop}	charge contribution due to the enrichment (or depletion) of the mobile dopant (acceptor or donor)
$\Sigma_{e'}$	charge contribution due to the enrichment (or depletion) of the electrons
Σ_i	charge contribution due to the enrichment (or depletion) of mobile charge carrier *i*
Σ_{SCL}	charge of the SCL
$\Sigma_{V_O^{\bullet\bullet}}$	charge contribution due to the enrichment (or depletion) of the oxygen vacancies
Φ , Φ_x	electric potential (at coordinate *x*)
Ω_i	reduced resistance change of the SCL in perpendicular direction concerning the transport of mobile charge carrier *i*

1.1 Numerical Method

In the following, we summarize the main equations of the numerical approach used to calculate the SCL charge carrier profiles. Please refer to Part I and the corresponding Supplementary Information for the detailed treatment and for a derivation of the relationships shown below.[1] A description of the physical quantities used here is given in Table 1.

The excess charge in the grain boundary core Σ_{Core} is compensated by two adjacent space charge layers (each with charge Σ_{SCL}).

$$\Sigma_{SCL} = -\frac{1}{2}\Sigma_{Core} \quad \{1\}$$

In the SCL, the mobile charge carrier concentrations c_i (*i* denotes an arbitrary mobile charge carrier) are rearranged compared with the bulk values $c_{i,\infty}$ according to

$$c_i = c_{i,\infty} \cdot e^{-\frac{z_i e}{k_B T}\Phi}, \quad \{2\}$$

where $k_B T$ is the Boltzmann term, *e* the elementary charge, z_i the corresponding charge number and Φ the electric potential arising from Σ_{Core}. For an arbitrary coordinate x_k (distance from the

boundary), the algorithm to numerically solve the Poisson-equation relies on the following expressions for the electric field E and the charge density ρ.[6]

$$E_{x_k} = \mathrm{sgn}\left(\Phi_{x_k}\right) \cdot \sqrt{\frac{2k_BT}{\varepsilon_r\varepsilon_0}\left(\sum_{i=1}^{N_M}\left(c_{i,x_k} - c_{i,\infty}\right) - \frac{\rho_{IM}}{k_BT}\Phi_{x_k}\right)} \quad \{3\}$$

$$\rho = e \cdot \sum_{i=1}^{N_M}\left(z_i c_i\right) + \rho_{IM}; \qquad \rho_{IM} = e \cdot \sum_{j=1}^{N_{IM}}\left(z_{IM,j} c_{IM,j}\right) \quad \{4\}$$

Here the subscript *M* refers to the mobile charge carriers and *IM* to the immobile ones.[III] At $x_0 = 0$, the concentrations $c_{i,0}$, the charge density ρ_0, and the electric field E_0 are determined using eq. {2} to {4}. Then, the spatial coordinate is increased by $x_k = x_{k-1} + \Delta x_k$, and the corresponding Φ_{x_k} is calculated according to the following Taylor approximation:

$$\Phi_{x_k} \approx \Phi_{x_{k-1}} + \Delta x_k \frac{d\Phi}{dx} + \frac{\Delta x_k^2}{2}\frac{d^2\Phi}{dx^2} + \frac{\Delta x_k^3}{6}\frac{d^3\Phi}{dx^3}, \quad \{5\}$$

from which

$$\Phi_{x_k} \approx \Phi_{x_{k-1}} - \Delta x_k \cdot E_{x_{k-1}} - \frac{\Delta x_k^2}{2\varepsilon_r\varepsilon_0}\left(\rho_{x_{k-1}} + \frac{\Delta\rho}{3}\right) \quad \{6\}$$

results. The potential value at the new coordinate allows for the determination of the electrical field E, the charge density ρ and the defect concentrations c_i there. The iteration of the described steps allows for the numerical computation of the SCL profile, i.e. the functions Φ(x), E(x), ρ(x) and all concentration profiles c_i(x). It is important recalling that as pointed out previously[1], Φ_0 is used here as input parameter for the calculation. Subsequently, in the light of the brick layer model,[8, 9] the effect of non-overlapping SCLs on the conductivity of a polycrystalline sample can be determined according to the following expressions:

$$s_{i,m} = \frac{\sigma_{i,m}}{\sigma_{i,\infty}} \quad \{7\}$$

[III] Concerning the immobile charge carriers, eq. {3} is based on the classical Mott-Schottky assumption of a flat dopant profile. It is noteworthy that in some cases the more complex situation of a frozen x-dependent concentration profile of an immobile dopant is realized. In the literature this situation was already considered, see e.g. ref. 7.

$$s_{i,m} = \left(\frac{4}{d} \cdot \frac{\Sigma_i}{z_i e c_{i,\infty}} + 1 \right) \cdot \frac{d}{2\Omega_i |z_i| e c_{i,\infty} + d} \quad \{8\}$$

$$\Sigma_i = z_i e \cdot \sum_{k=1}^{N_{Steps}-1} (c_{i,x_k} - c_{i,\infty}) \cdot \Delta x_k \quad \{9\}$$

$$\Omega_i = \frac{1}{|z_i| e} \cdot \sum_{k=1}^{N_{Steps}-1} \left(c_i^{-1} - c_{i,\infty}^{-1} \right) \cdot \Delta x_k \ . \quad \{10\}$$

Here $s_{i,m}$ is the effectively measured conductivity of the charge carrier i ($\sigma_{i,m}$) normalized with respect to the bulk conductivity ($\sigma_{i,\infty}$) including the influence of both parallel and perpendicular SCLs. Another important parameter is the total SCL charge Σ_{SCL}, which is the integrated charge density of the SCL. It can also be expressed as the sum of the individual charge contributions Σ_i of the mobile charge carriers:

$$\Sigma_{SCL} = \sum_{i=1}^{N_{mobile}} (\Sigma_i) \quad \{11\}$$

In order to quantitatively compare different SCL profiles, it is convenient to describe the profile shape by parameters such as the SCL extent ℓ_{SCL} and the SCL profile steepness α. The effective extent of the SCL is defined[1] here as the upper limit of the integration that is necessary to reach 99% of the charge Σ_i (or of Ω_i) (in contrast to the formal extent, i.e. the Debye-length λ (or 2λ) and the Mott-Schottky length λ^*):

$$r \cdot \Sigma_i = r \cdot z_i e \cdot \int_0^{\infty} (c_i - c_{i,\infty}) dx = z_i e \cdot \int_0^{\ell_{i,SCL}^{||}} (c_i - c_{i,\infty}) dx \quad \{12\}$$

$$r \cdot \Omega_i = \frac{r}{|z_i| e} \cdot \int_0^{\infty} (c_i^{-1} - c_{i,\infty}^{-1}) dx = \frac{1}{|z_i| e} \cdot \int_0^{\ell_{i,SCL}^{\perp}} (c_i^{-1} - c_{i,\infty}^{-1}) dx \quad \{13\}$$

with r equal to 0.99. Notably as the values of $\ell_{i,SCL}^{||}$ and $\ell_{i,SCL}^{\perp}$ can be different, the largest between them determines here the SCL extent ℓ_{SCL}.

The SCL steepness α can be defined as the ratio between the SCL extent ℓ_{SCL} and the charge balance point x_ρ, which is expressed as follows:

$$x_\rho = \frac{\int_0^{+\infty} x\rho \cdot dx}{\int_0^{+\infty} \rho \cdot dx} \approx \frac{\sum_{k=1}^{N_{Steps}-1} \left(x_k \cdot \rho_{x_k} \right)}{\Sigma_{SCL}} \quad \{14\}$$

$$\alpha = \ell_{SCL} / x_\rho \,. \quad \{15\}$$

This means that α is large for steep SCL profiles, in which the majority of the charge is located close to the boundary (low x_ρ value), whereas for SCL profiles characterized by a flat charge density α is small. [IV] The minimum value of α is 2 for a hypothetical, extremely flat, step-like charge density profile ($x_\rho = \frac{1}{2} \ell_{SCL}$).

2. Results and Discussion

2.1 Main features of the space charge layers

(i) Conductivity maps

The impact of the SCL effects on the overall ionic (left panel) and electronic (right panel) conductivity calculated according to the numerical method is shown again (cf. Part I) in **Fig. 1** for clarity.[V] The normalized effective conductivity $s_m = \sigma_m / \sigma_\infty$ is plotted as a function of the dopant concentration and Φ_0. The resulting conductivity change (z-axis) is color-coded (e.g. the green area represents a strong conductivity enhancement, the pink area a significant conductivity drop). In order to discuss the outcome of a possible adjustment of the SCL potential as experimentally attempted in several studies (see the introduction), a wide range of Φ_0 values was considered here. Therefore, the dopant concentration as well as the values of Φ_0 addressed here span over a range, which is clearly larger than those considered (or obtained) in previous contributions (ranging between 0.19 and 0.34 V [2, 10-14]; cf. also the area delimited by the blue rectangle in **Fig. 1**).

Notably, as illustrated in **Fig. 1**, the variations of σ_m with respect to σ_∞ do not only depend on Φ_0 but also on the dopant content. For a given potential, the conductivity change becomes smaller when the dopant concentration increases (e.g. s_m approaches unity).

[IV] A graphical example is given in Fig. S1 of the Supplementary Information of Part I.
[V] Note that the corresponding bulk concentrations are given in Fig. 4 of Part I.

The reason for the decreasing conductivity change with increasing dopant content stems from the fact that the charge carrier concentration profiles vary considerably with changing dopant concentration. It is instructive to consider a selection of profiles determined for constant potentials of -0.3 V and 0.3 V as illustrated in **Table 2**. They correspond to the positions marked by the white solid circles in **Fig. 1**, while the black circles with the white edge correspond to the profiles given in **Table 4** (obtained for a constant Σ_{SCL}).

It is important to note that for the following three situations the defect concentration of the enriched charge carrier exceeds the physical limit $c / c_{Ce} = 1$: (i) 20 mol% donor doped and $\Phi_0 = 0.3$ V, (ii) 1 mol% acceptor doped and $\Phi_0 = -0.3$ V, (iii) 20 mol% acceptor doped and $\Phi_0 = -0.3$ V. Such unrealistically high c / c_{Ce} ratios correspond to unrealistically large values of Σ_{SCL}. The role of Σ_{SCL} and, hence, the consequences arising from the impossibility to exceed realistic concentration values are discussed in Section 2.2.

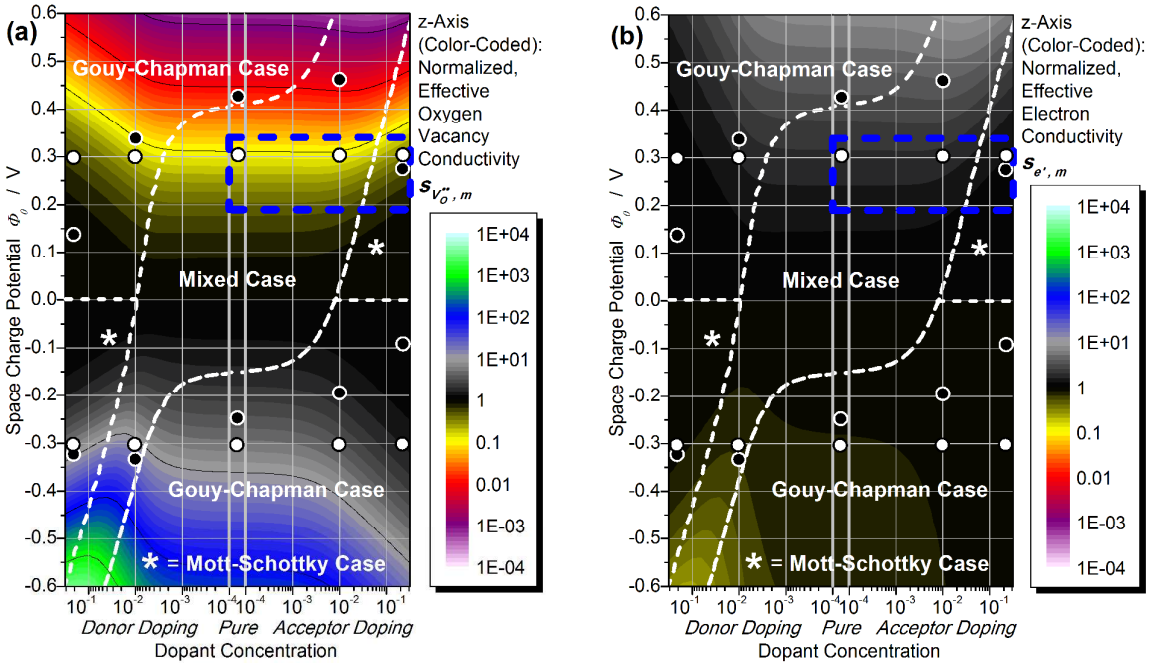

Fig. 1 Normalized effective conductivity $s_m = \sigma_m / \sigma_\infty$ of (a) the oxygen vacancies and (b) the electrons calculated with the numerical approach in a polycrystalline CeO_2 pellet with d = 40 nm as function of doping content and SCL potential. The s_m values plotted along the z-axis are color-coded. The blue rectangle indicates the potential values obtained in the literature. The circles locate the positions of the SCL profiles given in Table 2 (constant Φ_0, white solid circles) and Table 4 (constant Σ_{SCL}, black circles with white edge). The borders between the different cases are adopted from **Fig. 2a**.

Table 2 SCL profiles of constant potentials Φ_0 = 0.3 V and -0.3 V calculated using the numerical approach. The profiles correspond to the positions marked by the white solid circles in the contour plots of **Fig. 1** to **Fig. 3**, **Fig. 5** and **Fig. 6**.

20 mol% donor doped CeO_2 (z = 1)	1 mol% donor Doped CeO_2 (z = 1)	Pure CeO_2	1 mol% acceptor doped CeO_2 (z = -1)	20 mol% acceptor doped CeO_2 (z = -1)
$\Phi_0 = const = +0.3\ V$				
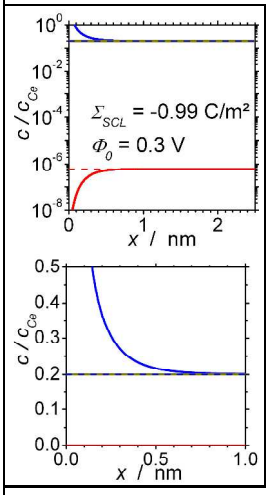	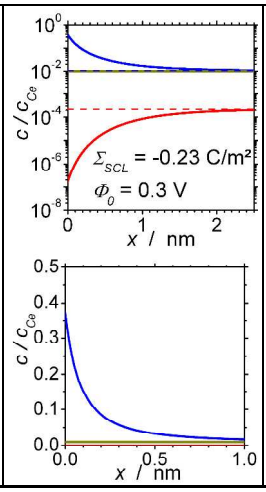	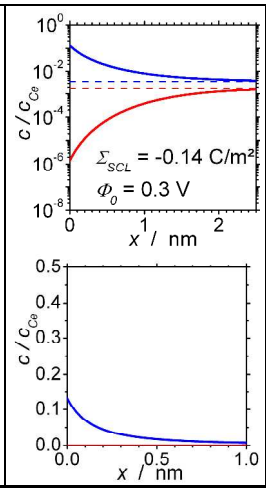	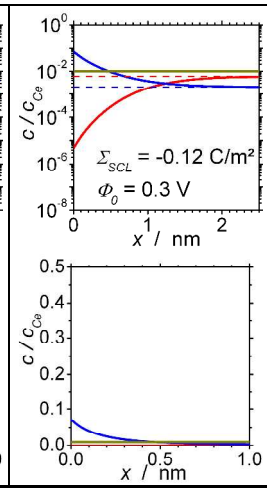	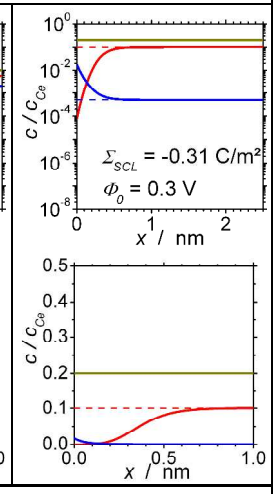
$\Phi_0 = const = -0.3\ V$				
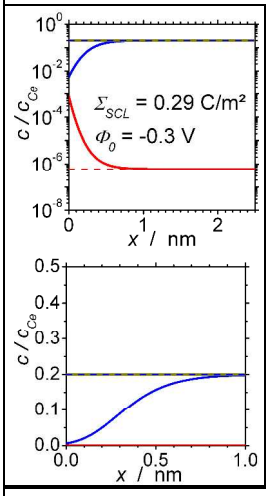	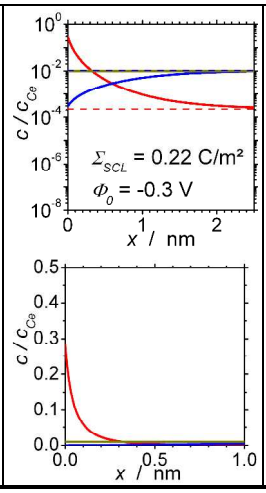	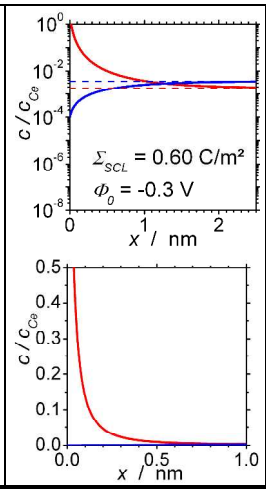	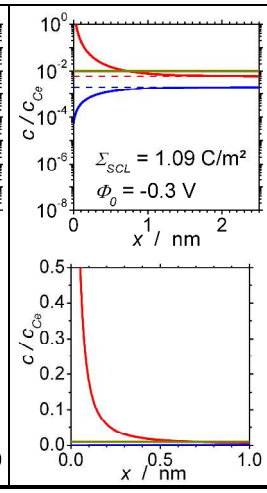	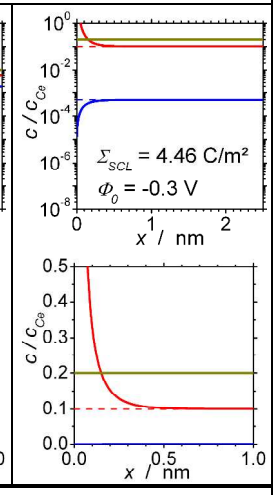
$V_O^{\cdot\cdot}$ e' Dopant $V_O^{\cdot\cdot}$ (bulk) e' (bulk)				

(ii) Charge compensation mechanism and SCL extent

From the profiles shown in **Table 2**, one can clearly recognize that, depending on the situation considered (e.g. dopant concentration, SCL potential), the net charge Σ_{Core} can be compensated in different ways. **Fig. 2** and **Fig. 3** visualize this aspect. Let us first consider the left panel of **Fig. 2**, where the ratio $\Sigma_{V_O^{\bullet\bullet}}/\Sigma_{SCL}$ is depicted as a function of Φ_0 and dopant concentration. Here, $\Sigma_{V_O^{\bullet\bullet}}/\Sigma_{SCL} \approx 1$ (white area) indicates a compensation of the core charge predominantly due to an enrichment (or depletion) of $V_O^{\bullet\bullet}$. For $\Sigma_{V_O^{\bullet\bullet}}/\Sigma_{SCL} \approx 0$ (black area), the core charge Σ_{Core} is compensated mainly by an enrichment (or depletion) of electrons. The grey areas represent mixed situations, in which concentration changes of both $V_O^{\bullet\bullet}$ and electrons contribute significantly to the compensation of Σ_{Core}. Notably, depending on Φ_0 and $\Sigma_{V_O^{\bullet\bullet}}/\Sigma_{SCL}$, 5 different compensation mechanisms can be identified as summarized in **Table 3**. The situations in which the SCL profiles are dominated by an enrichment or depletion of a single charge carrier so strongly that the counter charge carrier can be neglected are the well-known Gouy-Chapman and Mott-Schottky cases, respectively. All other cases in which both the enriched and the depleted charge carrier contribute significantly to Σ_{SCL} are here indicated as "mixed case".

Table 3 Charge compensation mechanisms defined as a function of Φ_0 and $\Sigma_{V_O^{\bullet\bullet}}/\Sigma_{SCL}$.

$\Phi_0 > 0$	$\Sigma_{V_O^{\bullet\bullet}}/\Sigma_{SCL} < 0.1$	Gouy-Chapman case (profiles dominated by the enrichment of electrons)
$\Phi_0 > 0$	$\Sigma_{V_O^{\bullet\bullet}}/\Sigma_{SCL} > 0.9$	Mott-Schottky case (profiles dominated by the depletion of oxygen vacancies)
$\Phi_0 < 0$	$\Sigma_{V_O^{\bullet\bullet}}/\Sigma_{SCL} < 0.1$	Mott-Schottky case (profiles dominated by the depletion of electrons)
$\Phi_0 < 0$	$\Sigma_{V_O^{\bullet\bullet}}/\Sigma_{SCL} > 0.9$	Gouy-Chapman case (profiles dominated by the enrichment of oxygen vacancies)
	$0.1 < \Sigma_{V_O^{\bullet\bullet}}/\Sigma_{SCL} < 0.9$	Mixed case (both oxygen vacancies and electrons contribute significantly to the total SCL charge)

It is important to stress here that the Gouy-Chapman and Mott-Schottky cases naturally result from the numerical calculations without the necessity of any assumption *a priori*. A great advantage of the numerical approach in comparison with the standard analytical models is given by the possibility to accurately describe the fairly large transition region between these two extreme cases, i.e. the grey colored area in **Fig. 2** (left) where $\Sigma_{V_O^{\bullet\bullet}}/\Sigma_{SCL} \approx \Sigma_{e'}/\Sigma_{SCL} \approx 1/2$.

The different shapes of the SCL profiles in the Gouy-Chapman and Mott-Schottky cases are visualized in the right panel of **Fig. 2** by using the profile steepness α. On the one hand, the GC-type profiles are characterized by a steep enrichment of charge carriers and a high concentration of the charge Σ_{SCL} very close to the interface (high steepness values increasing with $|\Phi_0|$). On the other hand, in the MS case the SCL profiles are dominated by the depletion of charge carriers which leads to a smoother distribution of the charge density Σ_{SCL} over the whole SCL extent. Hence, the steepness values are low and approach the minimum value of 2 of an ideal, step-like depletion profile.

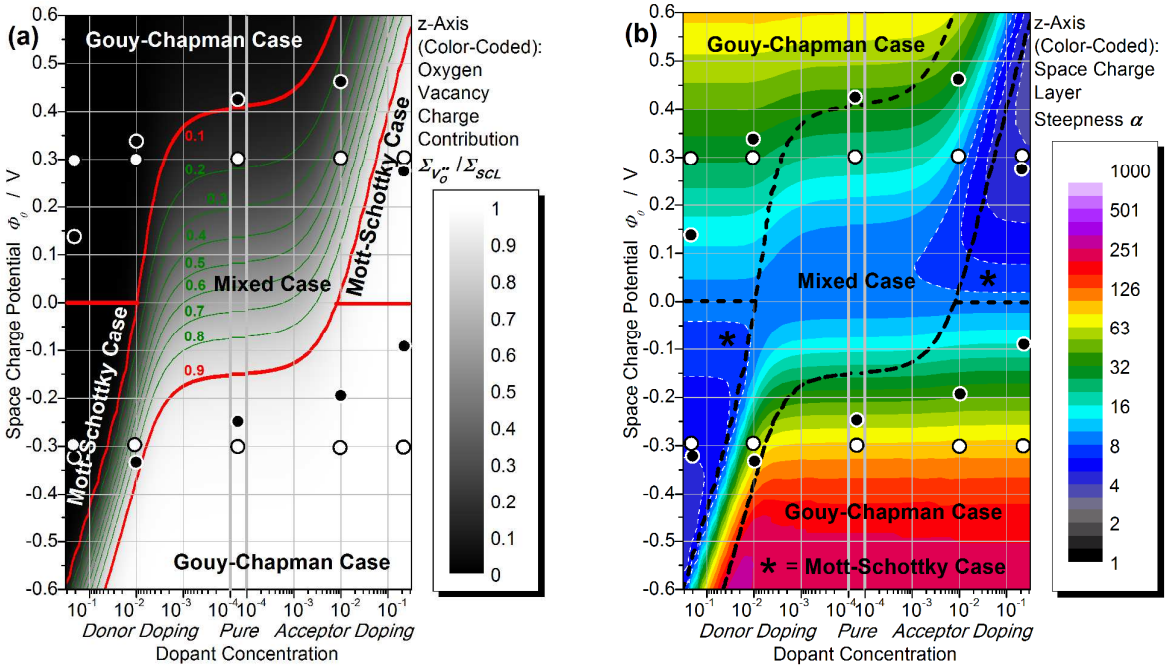

Fig. 2 Panel (a): relative contribution of the oxygen vacancies $\Sigma_{V_O^{\bullet\bullet}}/\Sigma_{SCL}$ to the total SCL charge. In the white areas, the SCL is dominated by an enrichment or depletion of oxygen vacancies; in the black areas by an enrichment or depletion of electrons. Panel (b): map of the SCL profile steepness α. While the Mott-Schottky profiles are characterized by a rather flat charge distribution (low α), the Gouy-Chapman type profiles are very steep since the majority of the SCL charge is located very close to the interface. Furthermore, the steepness of the Gouy-Chapman type profiles increases with increasing absolute potential value. For the Mott-Schottky type profiles, α decreases but cannot fall below the limit of 2 (the steepness of an ideal, flat step-like profile).

Another interesting feature of the SCL profile is its extension ℓ_{SCL} which is plotted in **Fig. 3a**. For the parameters used here the ℓ_{SCL} values are in the range between 0.4 and 5 nm. Given that $d = 40$ nm the assumption $d \gg \ell_{SCL}$ (non-overlapping SCLs) is fulfilled for all data points (under the conditions considered here). The fact that ℓ_{SCL} primarily depends on the bulk concentration (ℓ_{SCL} decreases with increasing dopant bulk concentration) explains the dopant content dependency of the conductivity at constant potentials as illustrated in **Fig. 1**. This is consistent with previous

experimental findings.[7, 15] Nonetheless, it is worth noting that, although the influence of the SCLs on the total conductivity decreases with increasing doping content, the numerical calculations show that for moderate potentials the SCL effects continue to significantly dominate the conductivity properties for heavily doped, nanocrystalline samples.

As far as the effect of the space charge potential on ℓ_{SCL} is concerned, it is worth recalling that the analytical approximations of the solution of the Poisson-equation lead to the following well-known conclusions: (1) In the Gouy-Chapman case for high potentials the SCL size (double Debye length 2λ) is independent of the potential and (2) in the Mott-Schottky case the SCL extension (the screening length λ^*) increases with increasing potential. The numerical calculations confirm that the outcome of the approximations are correct with one exception: Also in the Gouy-Chapman case, ℓ_{SCL} was found to slightly increase with increasing $|\Phi_0|$, particularly for very small potentials (cf. **Fig. 3**a).

By taking into account the dependencies of the SCL extent (**Fig. 3a)** and the SCL steepness (**Fig. 2b**), the rather complex dependencies of the conductivity change (**Fig. 1**) on the doping content and Φ_0 can be fully understood. As discussed above the decrease of the conductivity change for an increasing dopant level is a result of the decreasing SCL extend. Interestingly, for a given negative potential the oxygen vacancy conductivity shows a distinct maximum not for the undoped composition but for donor doping (e.g. see the green area at about 1 % donor doping for a potential of -0.6 V in **Fig. 1**, left panel). Also for positive potentials the conductivity decrease becomes maximal not for pure ceria but for acceptor doped material; here, however, the maximum is less distinct.

Remarkably, the origin of these maxima can be explained in terms of SCL steepness. For a given potential the defect concentration at the interface ($x = 0$) is fixed and, for steep profiles, the defect concentrations quickly reach the bulk values with increasing distance from the interface. Hence, the integral of such a profile results in a small conductivity change. On the contrary, for rather flat profiles, the defect concentrations deviate from the bulk values even over relatively large distances from the interface resulting in a larger net conductivity change. In conclusion, for a given potential the conductivity change within the SCL increases for decreasing α and increasing ℓ_{SCL} values. This situation is fulfilled best in the mixed case (compare **Fig. 2** with **Fig. 3a**) where indeed for a given Φ_0 the largest conductivity changes are observed (cf. also **Fig. 1)**.

This can also be well recognized by considering **Fig. 3b,** where the charge balance point $x_\rho = \ell_{SCL}/\alpha$ is plotted. Here, large values of x_ρ (corresponding to large ℓ_{SCL} and low α values) are in fairly good agreement with strong conductivity changes (**Fig. 1**) for a given potential.

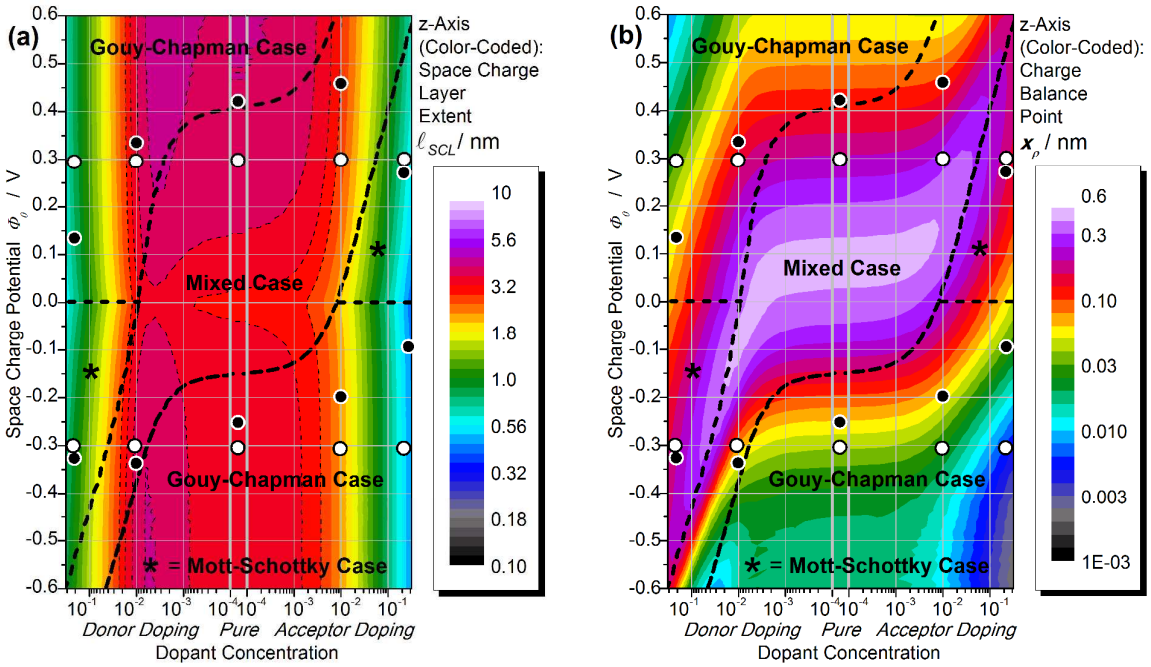

Fig. 3 (a) Extent of the SCL (ℓ_{SCL}) as a function of doping content and potential. The borders between the different cases are adopted from **Fig. 2a**. (b) Charge balance point x_ρ as a function of doping content and potential.

(iii) Influence of a mobile dopant

The conductivity maps presented above were calculated for an immobile dopant. It is now worth considering also the more complex case, in which the dopant cations can be rearranged under the influence of the SCL potential for example during sintering. It is important emphasizing that the resulting concentration profiles correspond to the equilibrium situation. The upper panels in **Fig. 4** show that the normalized conductivity (s_m) maps are in this case somewhat changed, with more symmetrically distributed conductivity values. The reason for this is shown in the charge distribution graph of **Fig. 4c**, in which the areas corresponding to the Mott-Schottky case of **Fig. 2a** are here dominated by the enrichment of the mobile dopant leading to typical Gouy-Chapman-like profiles. This effect can also be observed in the profile steepness plot of **Fig. 4d** where the α values in these areas are much higher compared with **Fig. 2b**. Due to this effect, in the regions of large dopant enrichment the influence of the SCLs on the conductivity is reduced compared with the immobile case.

Note that in **Fig. 4d** for donor doped ceria and negative potentials the steepness is still dependent on the dopant concentration. This results in a maximum of the conductivity increase (green area in **Fig. 4a**), which is similar to the one observed an immobile dopant (i.e. the green area in **Fig. 1a),** although here the maximum is less pronounced. The origin of this effect is the larger charge of the oxygen vacancies (+2) in comparison with the donor dopant (here +1) leading to an extremely steep enrichment of the oxygen vacancies in the SCL.

Obviously, charge carriers with large charges z_i perceive particularly strongly SCL effects (e.g. compare **Fig. 4a** with **Fig. 4b**). However, if the highly charged defects are enriched as majority charge carriers, the above described increase of the SCL steepness α partly compensates this effect. As an example, it is instructive to consider the case of pure ceria (see **Fig. 1a** or **Fig. 4a**). The conductivity increase for $\Phi_0 = 0.6$ V is more than three orders of magnitude and the concentration profiles are dominated by the enrichment of the singly charged electrons. For pure ceria and $\Phi_0 = -0.6$ V the doubly charged oxygen vacancies are enriched but their conductivity increase is significantly smaller than three orders of magnitude.

Such considerations indicate that one possible way to reduce the SCL effects on the conductivity (e.g. to reduce the drop of the ionic conductivity in acceptor doped ceria) can consist in using sufficiently mobile dopants, which, if possible, should be highly charged.[VI]

[VI] Note that in ref. 7 a similar case is discussed. Here, however, the mobility of the dopant is sufficient only at very elevated temperatures resulting in a "frozen" dopant profile at lower temperatures which complicates the situation considerably.

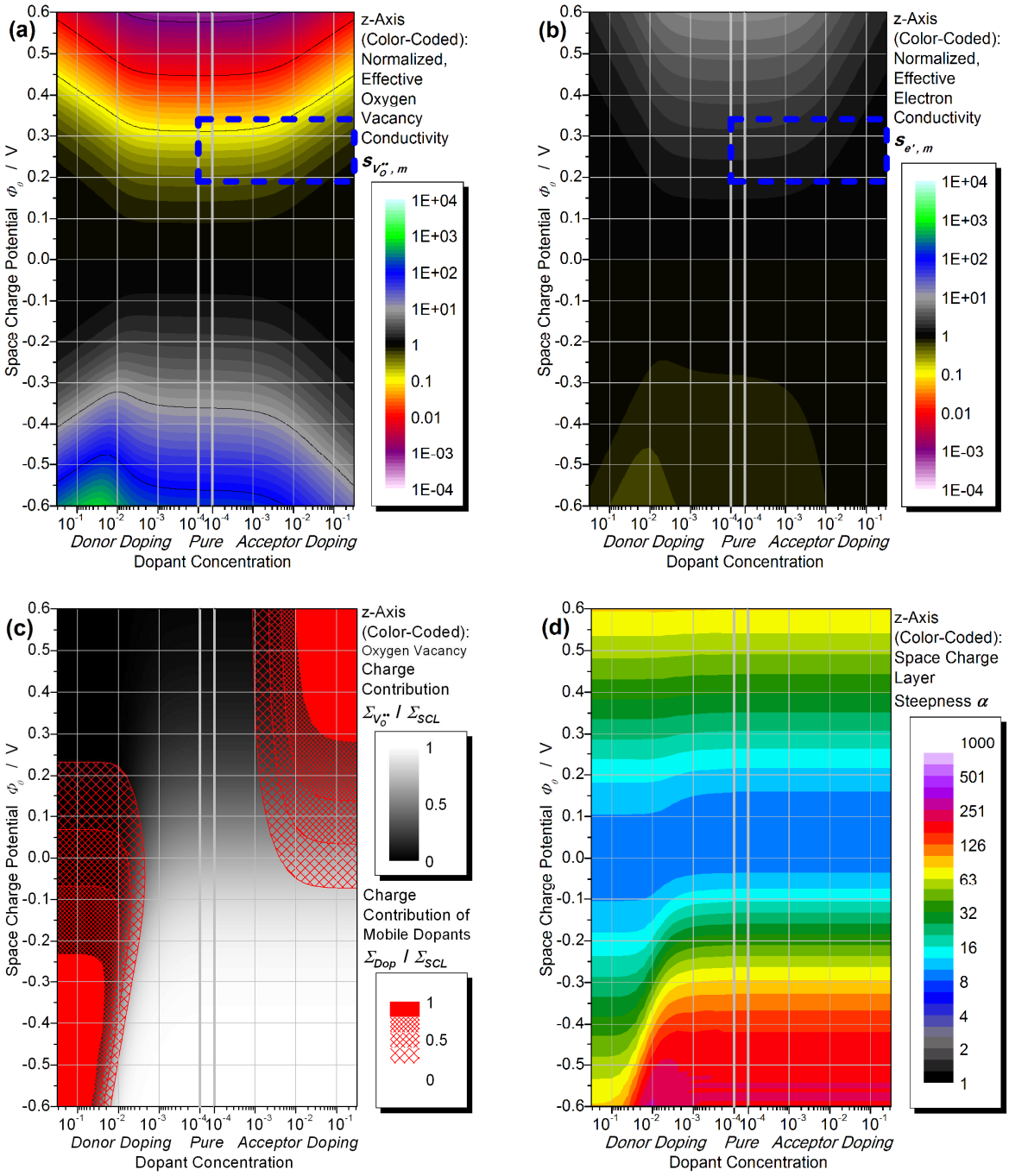

Fig. 4 The properties of the SCLs under the assumption of a mobile dopant. The top panels depict the normalized conductivity s_m maps for the (a) oxygen vacancies and (b) electrons. Panel (c): map of the charge contributions $\Sigma_{V_O^{\bullet\bullet}}/\Sigma_{SCL}$ (white and black areas), $\Sigma_{D^{\bullet}}/\Sigma_{SCL}$ and $\Sigma_{A'}/\Sigma_{SCL}$ (red areas). Panel (d): SCL steepness map.

2.2 Adjustment of the grain boundary core charge

In this section, we use the numerical calculations to study to which extent (under realistic conditions) the space charge effect could be adjusted to possibly enhance the conduction properties of nanocrystalline CeO_2. Before addressing this aspect, it is worth noting that usually, given the analytical approximations, as the ones shown in ref. 16, the conductivity changes are discussed as a function of the SCL potential. This is one of the main reasons why, with some exceptions, in most of the literature dealing with SCL effects in ionically and mixed conducting solids Φ_0 is used to characterize the SCL properties. On the one hand, this is of course practical, but on the other hand, this approach might be misleading, since it can give the impression that the electrical conduction properties could be drastically increased independently of other parameters if only the SCL potential can be modified. It is worth recalling here that the SCL potential Φ_0 only describes the defect concentration at the interface $c_{i,0}$ *relatively* to the bulk value $c_{i,\infty}$ and it is not an absolute quantity as Σ_{Core} (or Σ_{SCL}), which is instead constrained by microstructural reasons.[VII] In the following, it is shown that there are cases in which the adjustment of the grain boundary charge – e.g. by grain boundary decoration[4, 5, 18] – is useful, but also other situations, in which a substantial conductivity increase within the framework of the SCL theory is not possible.

For applications, such as solid oxide fuel cells (SOFCs), acceptor doped ceria is of key interest due to its high ionic conductivity. However, due to the positive SCL potential in polycrystalline material the ionic conductivity is severely reduced. Therefore, there is a strong interest towards adjusting the SCL properties and increase the ionic conductivity. Obviously, the extent to which one can improve the ionic conductivity is clearly limited by the extent to which one can modify Σ_{Core}. To get a rough estimate for the maximum value of $|\Sigma_{Core}|$ one can assume that half of the oxygen ions in one (100) plane of CeO_2 are missing. With the lattice constant of 5.41 Å, this yields an upper limit of $2 \cdot 2e/(5.41 \cdot 10^{-10}\text{m})^2 \approx 2\,\text{C/m}^2$. As Σ_{Core} is shielded by both sides of the GB (see eq. {1}), $|\Sigma_{SCL}| \leq 1\ \text{C/m}^2$ holds.

Using the numerical algorithm, it is possible to determine Σ_{SCL} as a function of the potential Φ_0 (**Fig. 5a**) and vice versa (**Fig. 5b**). Note that for $\Phi_0 > 0$ the negatively charged charge carriers are accumulated, leading to a negative value of Σ_{SCL} (and a positive Σ_{SCL} for $\Phi_0 < 0$). As shown in the graphs, the relationship between both parameters is rather complex: Quite remarkably, a high

[VII] The origin of space charge effects at grain boundaries stems from the fact that the charge carriers have different standard chemical potentials at the grain boundary core than in the bulk. Thus the SCL properties can be described in terms of standard chemical potentials as for example in ref. 17 in the case of CeO_2.

value of $|\Sigma_{SCL}|$ does not necessarily correspond to a high $|\Phi_0|$.[VIII] As an example, it is worth noting that, in **Fig. 5a**, for donor doped CeO_2 at a negative $\Phi_0 = -0.3\,\mathrm{V}$ the charge is about $0.2\ \mathrm{C/m^2}$ (at 1 % donor doping), whereas for the same potential in the acceptor doped material Σ_{SCL} increases far above the limit of $1\ \mathrm{C/m^2}$ leading to unrealistic situations (crossed area in the plot). Correspondingly, in **Fig. 5b**, for a charge of $0.4\ \mathrm{C/m^2}$ the potential is about $-0.5\,\mathrm{V}$ for donor doped but only approximately $-0.1\,\mathrm{V}$ for strongly acceptor doped ceria.

[VIII] In order to understand this finding, let us consider **Fig. 5**. For given temperature and Φ_0, i.e. a constant relative concentration change at the interface, the defect concentration of the majority charge carrier at the interface linearly increases with increasing bulk defect concentration (eq. {2}) and, hence, with increasing doping content. This increase overcompensates the corresponding decrease of ℓ_{SCL}, which is proportional to the square root of the doping content (cf. the Debye length λ) resulting in a net increase of the SCL charge with increasing doping content as displayed in **Fig. 5a**.
Furthermore, in contrast to the GC case, the local charge density in the MS case cannot exceed the charge density of the immobile dopant. Hence, for a given Φ_0, Σ_{SCL} is generally lower in the MS case compared with the GC case. As a result, for a given Φ_0, the lowest Σ_{SCL} values occur approximately at the border between the MS and the mixed case in **Fig. 5a** where a low dopant level coincides with a MS type profile. For a given potential the minimum of the SCL charge is, thereby, located at about the same dopant level where the conductivity effects are maximum (compare with **Fig. 1**). For this reason, if the conductivity is plotted versus the SCL charge (**Fig. 6**) very pronounced $s_{V_O^{\bullet\bullet},m}$ and $s_{e',m}$ maxima as well as asymmetrically distributed conductivity changes result.

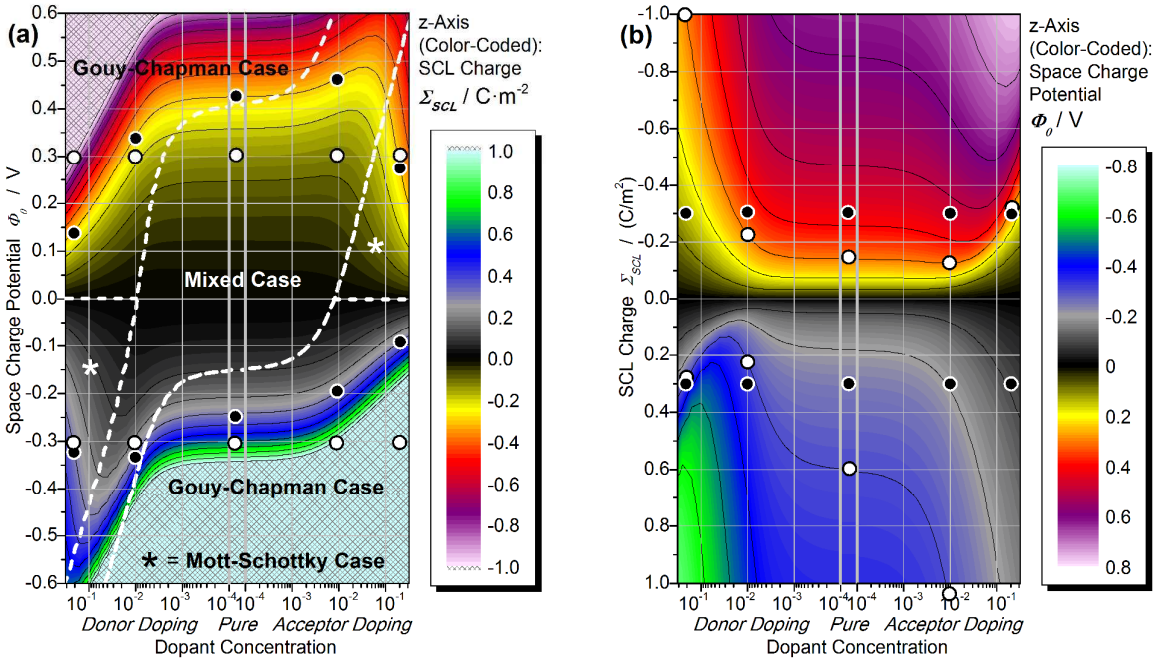

Fig. 5 Panel (a): SCL charge Σ_{SCL} as a function of SCL potential Φ_0 and doping content (The crossed area indicates unrealistically high charges $|\Sigma_{SCL}| > 1\ C/m^2$). Panel (b): SCL potential as function of SCL charge and doping content. Note that a positive Φ_0 corresponds to a negative Σ_{SCL} and vice versa. The circles indicate the positions of the SCL profiles given in **Table 2** (constant Φ_0, white solid circles) and **Table 4** (constant Σ_{SCL}, black circles with white edge).

These aspects are extremely relevant for the practical use of SCLs effects in CeO_2, since they reveal that in some cases the resulting improvement of the ionic conductivity can be rather limited. **Fig. 6** illustrates the conductivity change as a function of Σ_{SCL}. (Note that **Fig. 6** differs significantly from the charts in **Fig. 1,** see also footnote VII). The variations of conductivity are large for strongly acceptor doped materials and negative Σ_{SCL} (or donor doped and positive Σ_{SCL}). Thus a reduction of the negative charge (upper white arrow in **Fig. 6a**) could strongly improve the conductivity of nanocrystalline acceptor doped CeO_2 by orders of magnitude. However, this conductivity increase cannot exceed the bulk value (when Σ_{SCL} becomes zero). A further change of Σ_{SCL} towards positive values cannot enhance significantly the conductivity (lower white arrow in **Fig. 6a**) owing to the already high $V_O^{\bullet\bullet}$ concentration in the bulk. As an example, if we consider a 20 mol% acceptor doped CeO_2 bulk ($c_A = 5 \cdot 10^{21} cm^{-3}$), a large GB core charge of $-2\ C/m^2$ ($\Sigma_{SCL} = 1\ C/m^2$) and an average grain size $d = 40\ nm$, the concentration of $V_O^{\bullet\bullet}$ increases by only $3 \cdot 10^{20} cm^{-3}$. It is worth noting that alternatively, the same conductivity could be obtained by using an only slightly larger doping content of 22 mol% and $\Sigma_{Core} = 0$ (assuming that defect association effects can be neglected).

Let us now consider **Fig. 1a** again. Here it is shown that e.g. for 10 mol% acceptor doping $\Phi_0 = -0.5$ V leads to an increase of the $V_O^{\bullet\bullet}$ conductivity of one order of magnitude. However, as shown in **Fig. 5a** for such a Φ_0 value the resulting Σ_{SCL} exceeds the limit of 1 C/m^2. As a matter of fact, for 1 C/m^2 the Φ_0 value for 10 mol% acceptor doped ceria is only -0.2 V (**Fig. 5b**). For such values, the corresponding ionic conductivity $s_{V_O^{\bullet\bullet},m}$ is improved only slightly compared with the bulk value (**Fig. 1a**).

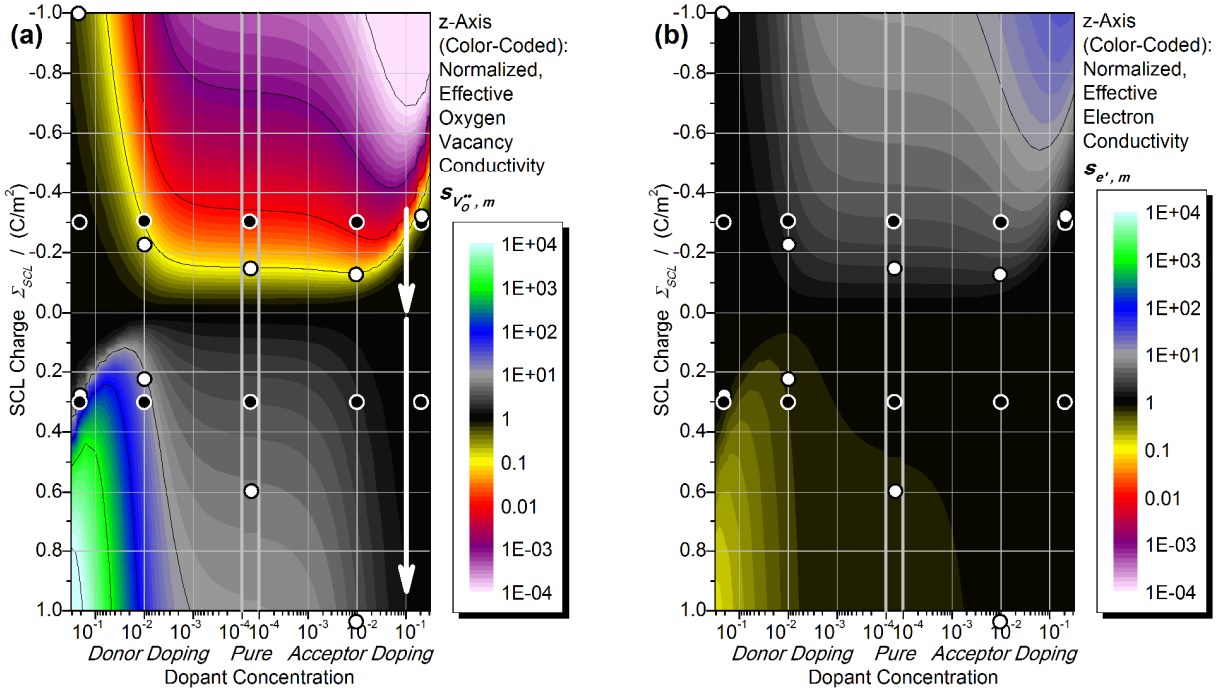

Fig. 6 Expected normalized conductivity s_m for the (a) oxygen vacancies and (b) electrons as a function of SCL charge Σ_{SCL} and doping content. The circles indicate the positions of the SCL profiles given in **Table 2** (constant Φ_0, white solid circles) and **Table 4** (constant Σ_{SCL}, black circles with white edge).

This effect can also be observed in the SCL profiles. In **Table 4**, characteristic profiles of constant SCL charge Σ_{SCL} are summarized. Note the differences compared with the profiles, which are obtained for a constant potential. (**Table 2)**. The profiles in **Table 2** are characterized by a constant relative conductivity change (i.e. the ratio c_0/c_∞ is constant, eq. {2}), as it can be observed in the logarithmic plots (since the relative conductivity change is independent of the absolute bulk value, the linear plots are quite different). The profiles with $\Sigma_{SCL} = const$ (**Table 4**) have instead rather similar linear plots with an identical area enclosed between the curves of c_i and $c_{i,\infty}$ (after having taken z_i

into consideration). Here it is the relative change (logarithmic plot) that differs between the spectra: For strongly acceptor doped ceria and a positive Σ_{SCL} the relative change is only very small. As a consequence, the adjustment of the SCLs in strongly doped materials can (i) certainly nullify the blocking character of the grain boundaries, but (ii) result in an overall ionic conductivity which exceeds the bulk conductivity only slightly. Nonetheless, it is worth emphasizing that for application purposes such effects would yet be extremely beneficial.

In addition, the fact that the SCL charge cannot exceed certain values (physical limits) is crucial for another fundamental aspect. The underlying relationship usually applied to deal with SCL effects is the Poisson-Boltzmann equation which, however, is restricted to diluted systems. Clearly, if both the bulk concentration and the SCL potential become too large, eq. {2} yields unrealistic concentration values above unity. In such situations also the SCL charge becomes extremely high (crossed areas in **Fig. 5a)**. On the contrary, in good approximation a low Σ_{SCL} indicates that the Poisson-Boltzmann equation is applicable (non-crossed areas in **Fig. 5a)**. This can also be observed in the SCL profiles shown in **Table 2** and **Table 4**. While for some of the profiles in **Table 2** (constant Φ_0 but in some cases very large Σ_{SCL}) the concentration exceeds unity, in the profiles of **Table 4** (constant and not too high SCL charge) this is not the case.

Table 4 SCL profiles of constant SCL charges $\Sigma_{SCL} = 0.3$ C/m² and -0.3 C/m² calculated using the numerical approach. The position of the profiles in the contour plots of **Fig. 1** to **Fig. 3**, **Fig. 5** and **Fig. 6**. is marked by the black circles with white edge.

20 mol% Donor Doped CeO_2 (z = 1)	1 mol% Donor Doped CeO_2 (z = 1)	Pure CeO_2	1 mol% Acceptor Doped CeO_2 (z = -1)	20 mol% Acceptor Doped CeO_2 (z = -1)
$\Sigma_{SCL} = const = -0.3\ C/m^2$				
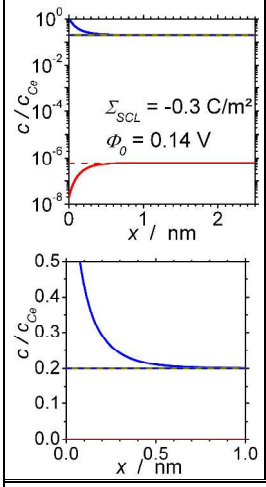	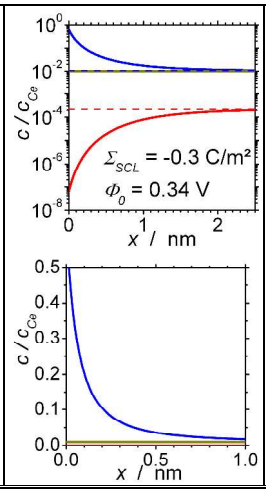	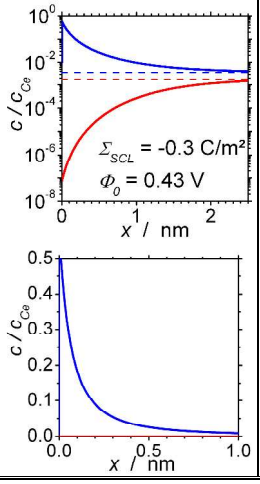	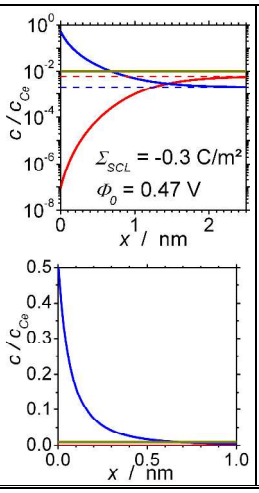	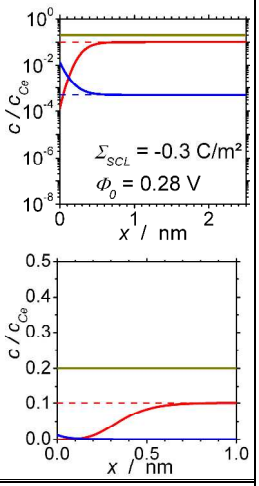
$\Sigma_{SCL} = const = +0.3\ C/m^2$				
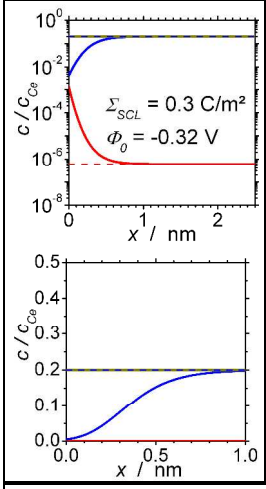	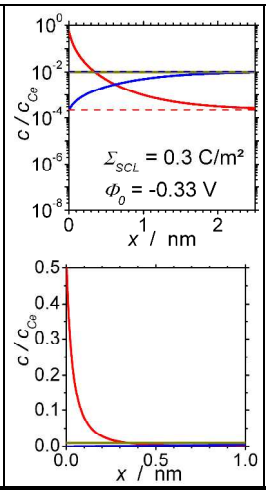	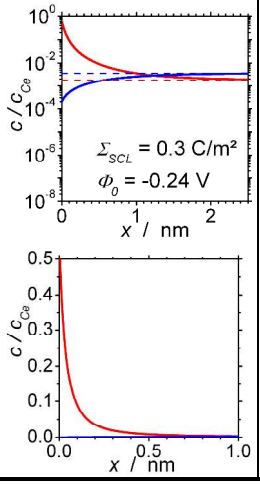	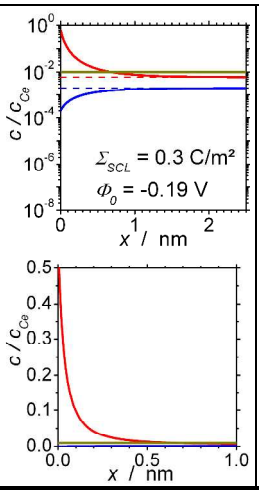	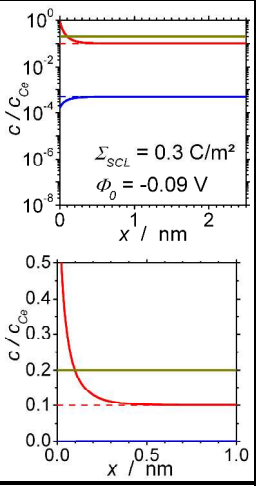
$V_O^{\cdot\cdot}$ e' Dopant $V_O^{\cdot\cdot}$ (bulk) e' (bulk)				

3 Summary

The numerical approach presented in Part I has been used here to investigate the main properties of the SCL profiles and the resulting conductivity effects in the case study of nanocrystalline ceria. Hereby a broad range of dopant concentration as well as space charge potential values has been considered. Furthermore, the role of a mobile dopant on the determination of the SCL profiles has been addressed. The complex relationships among the various SCL characteristics and their dependencies on the material parameters (doping content, defect equilibria, etc.) were discussed in detail. A summary of the main dependencies is given in Table 5.

Table 5 Schematic summary of the main dependencies of relevant SCL characteristics. Note that many of the given relationships are at a first glance rather intricate and sometimes even counteract each other.

The SCL conductivity effect increases	- with increasing absolute value of the SCL potential Φ_0. - with increasing SCL extent ℓ_{SCL}. - with decreasing SCL steepness α. - with increasing absolute value of the charge number z_i
The SCL extent ℓ_{SCL} increases	- with decreasing doping content/intrinsic bulk concentration. - with increasing absolute value of the SCL potential Φ_0 (in the MS case). - slightly with increasing absolute value of the SCL potential Φ_0 (in the GC case).
The SCL steepness α increases	- with increasing relative charge contribution of the enriched charge carrier (i.e. if the GC case and not the MS case applies). - with increasing absolute value of the SCL potential Φ_0 (in the GC case). - with decreasing absolute value of the SCL potential Φ_0 (in the MS case). - with increasing absolute value of the charge number of the enriched majority charge carrier (in the GC case).
The relative charge contribution Σ_i / Σ_{SCL} of the enriched charge carrier *i* increases (i.e. a MS case profile changes into a GC case profile)	- with increasing absolute value of the SCL potential Φ_0. - with decreasing dopant concentration (if the enriched charge carrier and the dopant are charged likewise). - if the mobility of the dopant is sufficient to follow the SCL potential and this dopant becomes the enriched majority charge carrier.
The SCL charge Σ_{SCL} increases	- with increasing absolute value of the SCL potential Φ_0. - with increasing doping content/intrinsic bulk concentration. - with increasing relative charge contribution of the enriched charge carrier (i.e. if the GC case and not the MS case applies). - with increasing absolute value of the charge number of the (enriched or depleted) majority charge carrier

Finally, the possibility of adjusting (under realistic conditions) the SCL effects to improve the conduction properties of nanocrystalline CeO_2 has been discussed. The results of the numerical analysis indicate that for strongly acceptor doped ceria a hypothetical enhancement of the ionic conductivity (oxygen vacancies) above the bulk value through an adjustment of the SCL potential to negative values is limited. Nonetheless, even if the bulk conductivity cannot be surpassed, the calculations show that already a reduction of the positive space charge potential can still result in a drastic ionic conductivity increase (given that for positive Φ_0 the oxygen vacancy transport can be strongly hindered at the grain boundaries, in some cases up to several orders of magnitude). A reduction of the positive SCL potential can thus be extremely beneficial for applications.

Acknowledgements

The authors would like to thank Uwe Traub of the Max Planck Institute for Solid State Research in Stuttgart for the IT support.

References

1. M. C. Göbel, G. Gregori and J. Maier, Physical Chemistry Chemical Physics, 2014 (This is Part I of the study)
2. S. J. Litzelman and H. L. Tuller, *Solid State Ionics*, 2009, **180**, 1190-1197.
3. H. Avila-Paredes and S. Kim, *Solid State Ionics*, 2006, **177**, 3075-3080.
4. G. Gregori, B. Rahmati, W. Sigle, P. A. van Aken and J. Maier, *Solid State Ionics*, 2011, **192**, 65-69.
5. P. Lupetin, F. Giannici, G. Gregori, A. Martorana and J. Maier, *Journal of the Electrochemical Society* 2012, **159**, B417-425.
6. R. Paul, *Halbleiterphysik,* Alfred Hüthig Verlag, Heidelberg 1983.
7. A. Tschöpe, S. Kilassonia and R. Birringer, *Solid State Ionics*, 2004, **173**, 57-61.
8. T. van Dijk and A. J. Burggraaf, *Phys. Stat. Sol. (a)*, 1981, **63**, 229-240.
9. J. Maier, *Ber. Bunsenges. Phys. Chem.* 1986, **90**, 26-33.
10. S. Kim and J. Maier, *Journal of the Electrochemical Society*, 2002, **149**, J73-J83.
11. M. C. Göbel, G. Gregori, X. Guo and J. Maier, *Physical Chemistry Chemical Physics*, 2010, **12**, 14351-14361.
12. A. Kossoy, Y. Feldman, E. Wachtel, K. Gartsman, I. Lubomirsky, J. Fleig and J. Maier, *Physical Chemistry Chemical Physic*, 2006, **8**, 1111-1115.
13. M. C. Göbel, G. Gregori and J. Maier, *Physical Chemistry Chemical Physics*, 2011, **13**, 10940-10945.
14. M. C. Göbel, G. Gregori and J. Maier, *J. Phys. Chem. C*, 2013, **117**, 22560−22568.
15. F. Maglia, F. Farina, M. Dapiaggi, I. G. Tredici and U. Anselmi-Tamburini, *Solid State Ionics*, 2012, **225**, 412-415.
16. S. Kim, J. Fleig and J. Maier, *Physical Chemistry Chemical Physics*, 2003, **5**, 2268-2273.
17. A. Tschöpe and R. Birringer, *Journal of Electroceramics*, 2001, **7**, 169-177.
18. S. J. Litzelman, R. A. De Souza, B. Butz, H. L. Tuller, M. Martin and D. Gerthsen, *Journal of Electroceramics*, 2009, **22**, 405-415.